JACS Au
AN OPEN ACCESS JOURNAL OF THE AMERICAN CHEMICAL SOCIETY

pubs.acs.org/jacsau
Letter

Isothermal Disorder-to-Order Transitions of DNA Origami Structures Induced by Alternative Component Subsets

Published as part of JACS Au special issue "DNA Nanotechnology for Optoelectronics and Biomedicine".

Yue Wang, Biancheng Wei, Qinglin Xia, Lei Ren, Bin Li, Linjie Guo, Ying Zhu, Lihua Wang,* Kai Jiao,* and Jiang Li*

Cite This: *JACS Au* 2025, 5, 1641−1648

Read Online

ACCESS | Metrics & More | Article Recommendations | Supporting Information

ABSTRACT: DNA origami technology has shown potential across various applications, including the construction of molecular machines. Among these, mimicking the complex structural transitions of natural biomolecules in physiological environments remains a long-standing pursuit. Here, inspired by intrinsically disordered proteins, we propose a strategy for inducing disorder-to-order transitions in DNA origami structures at room temperature using alternative component subsets. In a triangular DNA origami model, we define three subsets of its constitutional DNA staples based on their spatial distributions along the scaffold. Atomic force microscopy and molecular dynamics simulations show that the individual subsets result in metastable assemblies with disordered morphologies and elevated free-energy fluctuations compared with those generated by the complete set of staples. Notably, after the addition of the remaining staples, the irregular structures transform into ordered triangular architectures within 2 h at room temperature, achieving yields of up to ∼60%. These findings suggest that these controlled folding pathways in DNA origami can robustly converge on the global energy minimum at room temperature, thereby providing a promising alternative strategy for engineering biomimetic DNA molecular machines.

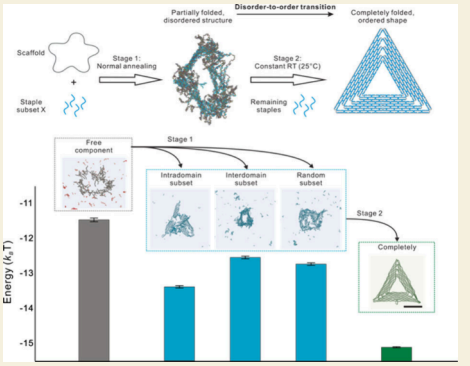

KEYWORDS: *DNA nanotechnology, DNA origami, self-assembly, isothermal assembly, molecular machines, structural transition*

Introduction. In recent decades, DNA nanotechnology has emerged as a versatile platform for the programmable fabrication of nanoarchitectures. Owing to its nanometer-scale programmability and addressability, DNA nanotechnology is driving innovations across diverse fields, including nanoelectronics, nanophotonics, biocomputing, biosensing, and biomedicine.[1−8] Particularly, it enables the fabrication of nanostructures that can be reconfigured postsynthesis, thereby holding promise for the development of molecular machines and nanorobots with dynamic structure−function transitions.[9−18] For example, a series of DNA nanorobots with openable nanocontainers have been engineered to release or expose their payloads in response to molecular stimuli, offering a promising platform for theranostic applications.[18−21] Despite prominent advancements, extending structural reconfiguration approaches for DNA nanostructures in physiologically compatible environments remains a long-standing pursuit.

Intrinsically disordered proteins (IDPs) make up a unique class of proteins characterized by their lack of a fixed or stable three-dimensional structure under physiological conditions. Despite their inherent flexibility, IDPs can undergo disorder-to-order transitions through a process known as induced folding. This transition is typically triggered by interactions with specific binding partners or changes in the cellular environment, allowing IDPs to adopt a more ordered conformation. This structural adaptability allows IDPs to participate in a wide range of cellular processes, including signal transduction, transcriptional regulation, and molecular recognition.[22] For example, the tumor suppressor p53,[23] a paradigmatic IDP, exhibits remarkable conformational plasticity that enables its functional responses to diverse cellular factors, including post-translational modifications,[24] metal ions,[25] and protein-binding partners such as MDM2.[26] The induced folding represents a transition from a metastable conformation with higher free energy to a stable conformation with lower free energy, which can provide inspiration for the development of novel molecular machines.

Here in this study, we seek to use DNA origami as a model system to mimic the disorder-to-order transition of IDPs via

Received: February 19, 2025
Revised: March 20, 2025
Accepted: March 24, 2025
Published: March 27, 2025

https://doi.org/10.1021/jacsau.5c00195
JACS Au 2025, 5, 1641−1648

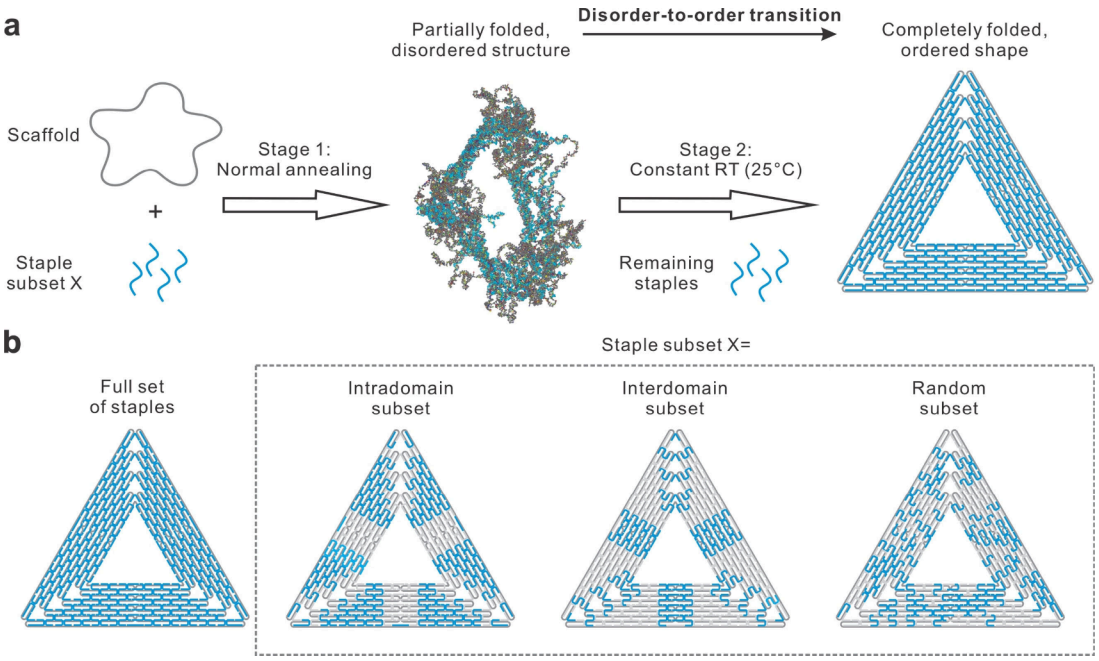

Figure 1. Scheme of the self-assembly of DNA origami with stepwise introduced subsets. (a) Flow diagram of the two-stage assembly. (b) Schematic illustration of the layouts of the staple subsets in triangular DNA origami. Blue lines, staples involved in the subsets.

induced folding in physiological environments. The DNA origami technique employs hundreds of single-stranded (ss-) DNAs (staples) to induce the folding of a long ssDNA scaffold (typically M13 bacteriophage DNA) into prescribed shapes via Watson−Crick base pairing.[1] This process is somewhat analogous to protein folding. However, in contrast to the rapid protein folding that occurs under physiological conditions, conventional DNA origami folding requires an activation step involving heating to denaturing temperatures to avoid kinetic traps. Recent reports indicate that this folding process can also occur at room temperature[27−31] but requires denaturing agents or extremely long assembly times (at least 24 h). Here, to address this challenge, we divided the staples of the triangular DNA origami structure into subsets. We utilized certain subsets to prefold the scaffold partially, generating flexible, irregular structures akin to IDPs. Subsequently, we induced the disorder-to-order transition of these structures at room temperature in 2 h using the remaining staples.

Results and Discussion. In this study, we employed a previously described triangular DNA origami structure as the model structure[1] (detailed in Figure S1 and Supporting Information Experimental section). It is composed of six right-angled trapezoidal domains generated along the scaffold folding pathway. Within each domain, the scaffold is folded antiparallel by intradomain staples. The U-turns of the folded scaffold delineate the edges of each domain, which are bridged by interdomain staples that cohesively integrate the six domains into a closed triangular framework.

To mimic the disorder-to-order transition of IDPs, we designed an unconventional self-assembly process of adding staples in two stages (Figure 1a). In Stage 1, we selected a portion of a full set of DNA staples (207 staples) as a subset to be added to the assembly solution containing scaffold for conventional annealing assembly (heating to 80 °C for 3 min and then annealing at 0.5 °C/min to 25 °C). In Stage 2, the remaining staples (i.e., the complement of the above subset) were added to the above assembly system and incubated isothermally at 25 °C for 120 min. We expected that Stage 1 would produce partially folded, relatively flexible, and disordered structures. However, under room-temperature conditions (25 °C) and at the conventional salt concentration (12.5 mM Mg^{2+}) of DNA origami of a complete set, the assembly of DNA origami structures is susceptible to kinetic traps that lead to structural disorder.[32−34] To ensure the correct formation of DNA origami structures, it is often necessary to heat the sample to the denaturation temperature (e.g., 95 °C for 3 min[1] or 65 °C for 15 min[35]) to unfold incorrect structures. Here, we sought to investigate whether partial folding of the scaffold during Stage 1 can activate the scaffold. We also asked the question of whether these structures can rapidly transition to fully folded, ordered, and rigid triangular origami structures at room temperature during Stage 2, thereby achieving a disorder-to-order transition similar to that induced by IDPs.

Based on the spatial distribution of staples on the structure of DNA origami products,[36] we set up three subsets of staples (Figure 1b, Tables S1−S4): (1) Intradomain subset. As shown in the schematic, this subset has 123 staples that span close distances on the scaffold and are located inside the structural domains of the triangular origami. (2) Interdomain subset. This subset, containing 84 staples, is a complement to the intradomain subset. They span long distances on the scaffold and serve as interdomain linkers in the structure (Figure S1). (3) Random subset. This set comprises 104 randomly selected staples (50% of the full set), which are randomly distributed across the DNA origami structure. We expect that different distributions of the staple subset can produce Stage 1 products with various morphologies and free energy levels and affect their efficiency in generating target structures in Stage 2.

Next, we used molecular dynamics simulations and experiments to investigate the structural morphologies of DNA origami structures resulting from different staple subsets in Stage 1 (Figure 2a). We used oxDNA (see Supporting Information for details) to construct coarse-grained models of

https://doi.org/10.1021/jacsau.5c00195
JACS Au 2025, 5, 1641−1648

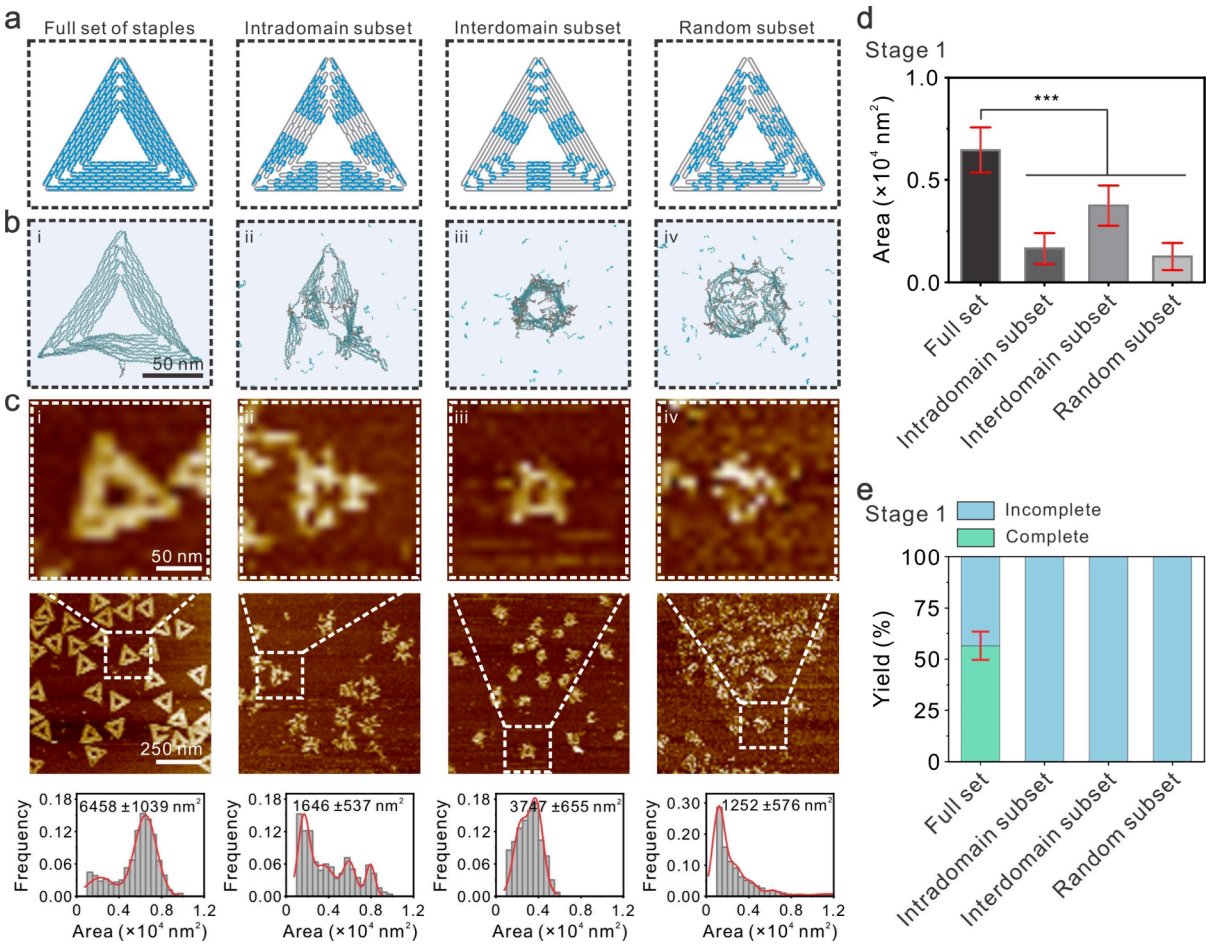

Figure 2. Partially folded DNA origami structures resulting from different subsets. (a) Schematic of the layouts of different staple subsets in DNA origami structures in Stage 1; (b) Snapshots of coarse-grained molecular dynamics simulations of different staple subset products from Stage 1. (c) Representative AFM images of different subset products from Stage 1, and the area distribution statistics of the monolithic structure (N ≈ 1000 structures). Red solid lines are GaussAmp fitting. (d) Histogram of the area distribution of monomer structures of different subset products from Stage 1 (N ≈ 1000 structures). (e) Yield statistics for uncompleted structures of different subsets from Stage 1. Data are presented as mean ± s.d. (N ≈ 1000 structures). ***, $p < 0.001$, analyzed with one-way ANOVA.

the Stage 1 products,[37] by placing the staple subsets in their prescribed positions within the DNA origami structure. Both the simulation snapshots (Figure 2b) and their experimental results in AFM images (Figure 2c, Figures S2−S5) show that the four Stage 1 products exhibit morphologies distinct from each other. For each product, the morphology observed via AFM generally corresponds with the simulation prediction. In detail, (i) the full set of staples, as the normal control, led to complete triangular shapes as prescribed. The mean area per structure, as determined from AFM images, was 6458 ± 1039 nm^2. (ii) The intradomain subset led to irregular structures (mean area, 1646 ± 537 nm^2). They were characterized by multiple separate structural domains lacking fixed positions and orientations, suggesting that the interdomain connections are flexible. This flexibility is attributed to the absence of multiple interdomain staples. (iii) The interdomain subset led to irregular shrunken shapes (mean area 3747 ± 655 nm^2) compared to the complete triangular shape. This could be due to the lack of intradomain staples to fill the structure. The results suggest that although interdomain folding is generally considered more difficult than intradomain folding, the combined effects of an annealing process initiated at the denaturation temperature, the structural flexibility of the scaffold, and the synergistic action of multiple staples still enable effective interdomain folding even in the presence of only interdomain staples. (iv) The random subset, on the other hand, resulted in more irregular shapes (1252 ± 576 nm^2), devoid of distinct structural features, which could be attributed to the random distribution of the staples. Collectively, all three structures (ii-iv) derived from partial staples exhibited smaller sizes compared to those from the full set of staples (i) (Figure 2d). Under our conditions, the full staple set resulted in complete triangular structures with a yield of ∼56.5%, whereas the three subsets did not yield any complete triangles (Figure 2e).

Subsequently, we examined whether the metastable products in Stage 1 can be further folded into complete triangle structures at room temperature. We supplemented the remaining staples for the Stage 1 products and allowed them to react at room temperature for 120 min (i.e., Stage 2). The AFM results (Figure 3a) show that all three samples, originally derived from intradomain, interdomain, and random subsets, resulted in a large fraction of complete triangular structures in Stage 2 under our room-temperature conditions. Meanwhile, we observed some incompletely folded structures similar to those in Stage 1 (marked by the white dashed circles in Figure 3a). The mean areas per structure, measured from AFM images, were 7002 ± 987, 5870 ± 926, and 5377 ± 1237 nm^2,

https://doi.org/10.1021/jacsau.5c00195
JACS Au 2025, 5, 1641−1648

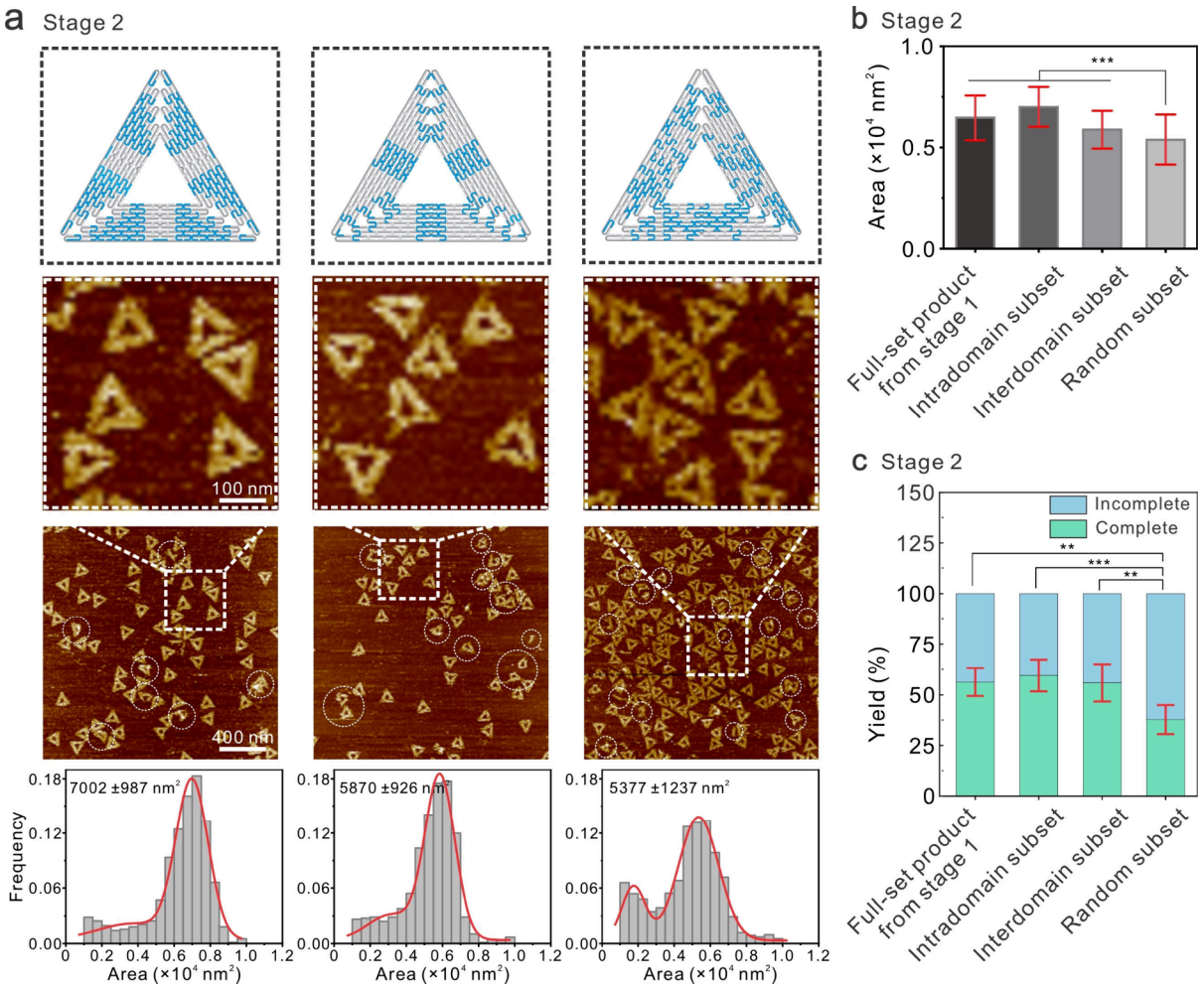

Figure 3. Complete DNA origami structures resulting from different pathways. (a) Schematic of the different subset types in Stage 2, the assembled AFM results, and the statistical analysis of the area of monolithic structures (N ≈ 1000 structures). White dashed circles, incomplete shapes. (b) Histogram of the statistical analysis of the area of monolithic structures produced by the different Staple subsets in Stage 2 (N ≈ 1000 structures). (c) Yield statistics for complete structures of each subset in Stage 2. Red solid lines, GaussAmp fitting. Data are presented as mean ± s.d. (N ≈ 1000 structures). **, $p < 0.01$; ***, $p < 0.001$, analyzed with one-way ANOVA.

respectively (Figure 3b, Figures S6–S8). The yields of complete triangles, originated from the intradomain, interdomain, and random subsets, were approximately 59.6%, 55.9%, and 37.8%, respectively (Figure 3c). Among them, the intradomain and interdomain subsets led to areas per structure with yields similar to those derived from the normal assembly approach with the full staple set (6458 ± 1039 nm^2 and 56.5%). In comparison, the random subset led to a generally smaller product area and thus the lowest yield of complete triangles. Indeed, we observed more defects in the structures that originated from the random subset in the AFM images. These results suggest that compared to the random staple distribution, the distributions of intradomain and interdomain subsets in Stage 1 products are more favored by further assembly under isothermal conditions.

To further interpret our observations in terms of free energy landscapes, we evaluated the equilibrium free energy levels of the structures derived from the molecular dynamics simulations (Figure 4a-c). The results show that the free scaffold and staples in the initial state have the highest free energy (−11.51 k_BT), whereas the fully folded, complete triangle structure in the final state exhibits the lowest free energy level (−15.10 k_BT). The three Stage 1 products, resulting from intradomain, interdomain, and random subsets, exhibit energy levels of −13.39, −12.54, and −12.73 k_BT, respectively (Figure 4b). These values confirm that these are metastable structures with free energy levels situated between the initial free components and complete triangles. Among the three subsets, the intradomain subset led to the lowest energy state, in agreement with previous studies showing that staples across short distances on the scaffold are more favored than interdomain staples.[36,38] In addition, the Stage 1 products that resulted from intradomain, interdomain, and random subsets show higher free energy standard deviations (S.D.) (0.033, 0.037, and 0.038 k_BT, respectively) compared to the complete triangle structure (0.017 k_BT). These results suggest that the partially folded Stage 1 products have higher free energy fluctuations than the complete structure, which could be attributed to their flexible and dynamic conformations.

Overall, the simulation results are in agreement with the experimental observations. These findings suggest that products generated in Stage 1 adopt partially folded, flexible conformations residing in metastable fluctuating energy states. The distinct distributions of the staple subsets on the scaffold account for the observed variability in energy levels. Following the Stage 2 reaction—where the remaining staples are

https://doi.org/10.1021/jacsau.5c00195
JACS Au 2025, 5, 1641−1648

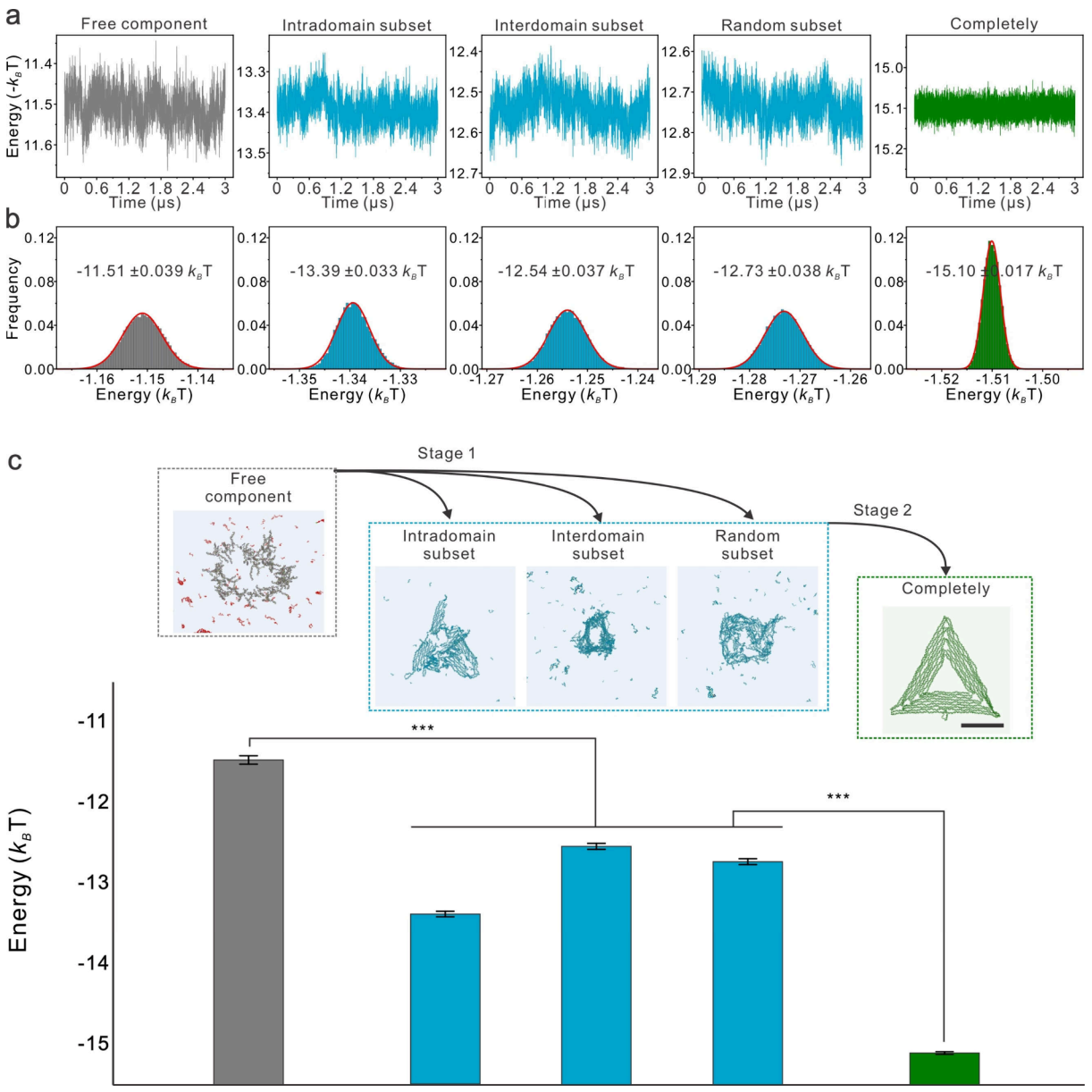

Figure 4. Simulated free energy landscapes resulting from different subsets. (a) Energy equilibrium oscillation curves of the free energies of the structures of different subsets; (b) Energy frequency distributions of the free energies of the structures of different subsets; (c) Energy histograms of the structures at different stages of the folding process for each set type; gray denotes the initial unfolded state; blue denotes the different structures generated by the folding of the different subset staples; and green denotes the completed shapes. Scale bar: 50 nm. The free energies of the structures are in units of k_BT, where k_B is the Boltzmann constant, and T is the absolute temperature. Data are presented as mean ± s.d. (N ≈ 20,000 samplings in a simulation). ***, $p < 0.001$, analyzed with one-way ANOVA.

introduced at room temperature—these intermediates transition into fully folded structures corresponding to a global energy minimum.

Conclusions. In summary, we demonstrate in this study the disorder-to-order transitions of DNA origami structures at room temperature. By employing various subsets of staples, we obtained metastable structures characterized by irregular morphologies and fluctuations in free energy levels. These structures, upon induction by the complement staples, robustly folded into well-defined triangular configurations within 2 h at room temperature, achieving substantial yields.

Previous studies indicate that in one-pot self-assembly, the folding cooperativity[36,39,40] domains guide the multidomain DNA origami predominantly following a folding pathway where intradomain folding precedes interdomain stitching.[34,36,41,42] This study introduces artificially defined folding pathways through the sequential addition of staple subsets including interdomain and random subsets. These pathways may be energetically unfavorable compared to those naturally selected in the one-pot method. However, these unconventional pathways still achieve the global energy minimum state at a considerable rate under isothermal conditions at room temperature, to some degree, analogous to the induced folding of IDPs. We reason that this capability largely stems from the partial folding products of Stage 1, which exert an "activating effect" on the scaffold, resulting in a molecular conformation conducive for further folding.[43,44] Indeed, other studies have found that such loose nucleic acid folding conformations

https://doi.org/10.1021/jacsau.5c00195
JACS Au 2025, 5, 1641−1648

facilitate the binding of external molecules.[45,46] Our previous investigations also indicate that, in the absence of Stage 1 activation by these subsets, the room-temperature assembly can rarely yield prescribed DNA origami structures within a short period.[32,33] While existing DNA molecular machines allow dynamic structural reconfiguration at constant/ambient temperatures through approaches such as strand displacement reactions, hydrophobic interactions, and ion-induced aggregation,[6,9−11,47] they typically respond to a very limited number of stimuli, resulting in a restricted diversity of morphological changes. In contrast, the strategy presented in this study can respond to combinations of hundreds of nucleic acid sequences. Given that DNA origami technology can fold into various shapes using the same scaffold sequence with different staple combinations, this method theoretically enables more flexible and diverse structural transformations, leading to more complex functional state transitions.

Future research could focus on broadening the applicability of this strategy. This could involve designing a wider array of staple subsets to induce more diverse structural transformations, thereby enabling complex functional state transitions. This has potential value for applications in high-throughput molecular computing, information storage, and biological diagnostics under ambient conditions.

■ ASSOCIATED CONTENT

Supporting Information

The Supporting Information is available free of charge at https://pubs.acs.org/doi/10.1021/jacsau.5c00195.

Layout of DNA origami structure, AFM images, staple IDs of staple subsets, DNA sequences, experimental section, additional references (PDF)

■ AUTHOR INFORMATION

Corresponding Authors

Lihua Wang − *Institute of Materiobiology, College of Sciences, Shanghai University, Shanghai 200444, China; Shanghai Collaborative Innovation Center of Intelligent Sensing Chip Technology, Shanghai University, Shanghai 200444, China;* orcid.org/0000-0002-6198-7561; Email: wanglihua@shu.edu.cn

Kai Jiao − *Institute of Materiobiology, College of Sciences, Shanghai University, Shanghai 200444, China;* Email: kjiao@shu.edu.cn

Jiang Li − *Institute of Materiobiology, College of Sciences, Shanghai University, Shanghai 200444, China;* orcid.org/0000-0003-2372-6624; Email: lijiang80@shu.edu.cn

Authors

Yue Wang − *Division of Physical Biology Department, CAS Key Laboratory of Interfacial Physics and Technology, Shanghai Institute of Applied Physics, Chinese Academy of Sciences, Shanghai 201800, China; University of Chinese Academy of Sciences, Beijing 100049, China*

Biancheng Wei − *Division of Physical Biology Department, CAS Key Laboratory of Interfacial Physics and Technology, Shanghai Institute of Applied Physics, Chinese Academy of Sciences, Shanghai 201800, China; University of Chinese Academy of Sciences, Beijing 100049, China*

Qinglin Xia − *Division of Physical Biology Department, CAS Key Laboratory of Interfacial Physics and Technology, Shanghai Institute of Applied Physics, Chinese Academy of Sciences, Shanghai 201800, China; University of Chinese Academy of Sciences, Beijing 100049, China*

Lei Ren − *Division of Physical Biology Department, CAS Key Laboratory of Interfacial Physics and Technology, Shanghai Institute of Applied Physics, Chinese Academy of Sciences, Shanghai 201800, China; University of Chinese Academy of Sciences, Beijing 100049, China*

Bin Li − *Division of Physical Biology Department, CAS Key Laboratory of Interfacial Physics and Technology, Shanghai Institute of Applied Physics, Chinese Academy of Sciences, Shanghai 201800, China; University of Chinese Academy of Sciences, Beijing 100049, China;* orcid.org/0000-0002-8348-7445

Linjie Guo − *Institute of Materiobiology, College of Sciences, Shanghai University, Shanghai 200444, China;* orcid.org/0009-0005-1159-3280

Ying Zhu − *Institute of Materiobiology, College of Sciences, Shanghai University, Shanghai 200444, China;* orcid.org/0000-0003-0418-919X

Complete contact information is available at: https://pubs.acs.org/10.1021/jacsau.5c00195

Author Contributions

CRediT: **Yue Wang** conceptualization, data curation, formal analysis, investigation, visualization, writing - original draft; **Biancheng Wei** investigation, methodology; **Qinglin Xia** investigation, methodology; **Lei Ren** investigation, methodology; **Bin Li** methodology, supervision, validation, visualization; **Linjie Guo** formal analysis, validation, visualization, writing - review & editing; **Ying Zhu** project administration, resources, supervision, writing - review & editing; **Lihua Wang** project administration, resources, supervision, writing - review & editing; **Kai Jiao** project administration, supervision, writing - review & editing; **Jiang Li** conceptualization, funding acquisition, project administration, supervision, writing - review & editing.

Notes

The authors declare no competing financial interest.

■ ACKNOWLEDGMENTS

This work was supported by the National Key Research and Development Program (2020YFA0908900) and the National Natural Science Foundation of China (22325406, 32301185, 22204100).

■ REFERENCES

(1) Rothemund, P. W. K. Folding DNA to Create Nanoscale Shapes and Patterns. *Nature* **2006**, *440* (7082), 297−302.

(2) Douglas, S. M.; Dietz, H.; Liedl, T.; Högberg, B.; Graf, F.; Shih, W. M. Self-Assembly of DNA into Nanoscale Three-Dimensional Shapes. *Nature* **2009**, *459* (7245), 414−418.

(3) Hong, F.; Zhang, F.; Liu, Y.; Yan, H. DNA Origami: Scaffolds for Creating Higher Order Structures. *Chem. Rev.* **2017**, *117* (20), 12584−12640.

(4) Liu, X. G.; Zhang, F.; Jing, X. X.; Pan, M. C.; Liu, P.; Li, W.; Zhu, B. W.; Li, J.; Chen, H.; Wang, L. H.; Lin, J. P.; Liu, Y.; Zhao, D. Y.; Yan, H.; Fan, C. H. Complex Silica Composite Nanomaterials Templated with DNA Origami. *Nature* **2018**, *559* (7715), 593−598.

(5) Dey, S.; Fan, C.; Gothelf, K. V.; Li, J.; Lin, C.; Liu, L.; Liu, N.; Nijenhuis, M. A. D.; Saccà, B.; Simmel, F. C.; Yan, H.; Zhan, P. DNA Origami. *Nat. Rev. Methods Primers* **2021**, *1* (1), 13.

(6) Li, J.; Green, A. A.; Yan, H.; Fan, C. H. Engineering Nucleic Acid Structures for Programmable Molecular Circuitry and Intracellular Biocomputation. *Nat. Chem.* **2017**, *9* (11), 1056−1067.
(7) Lv, H.; Xie, N. L.; Li, M. Q.; Dong, M. K.; Sun, C. Y.; Zhang, Q.; Zhao, L.; Li, J.; Zuo, X. L.; Chen, H. B.; Wang, F.; Fan, C. H. DNA-Based Programmable Gate Arrays for General-Purpose DNA Computing. *Nature* **2023**, *622* (7982), 292−300.
(8) Yin, F.; Zhao, H.; Lu, S.; Shen, J.; Li, M.; Mao, X.; Li, F.; Shi, J.; Li, J.; Dong, B.; Xue, W.; Zuo, X.; Yang, X.; Fan, C. DNA-Framework-Based Multidimensional Molecular Classifiers for Cancer Diagnosis. *Nat. Nanotechnol.* **2023**, *18* (6), 677−686.
(9) Yurke, B.; Turberfield, A. J.; Mills, A. P., Jr; Simmel, F. C.; Neumann, J. L. A DNA-Fuelled Molecular Machine Made of DNA. *Nature* **2000**, *406* (6796), 605−608.
(10) Zhang, D. Y.; Seelig, G. Dynamic DNA Nanotechnology Using Strand-Displacement Reactions. *Nat. Chem.* **2011**, *3* (2), 103−113.
(11) Nummelin, S.; Shen, B.; Piskunen, P.; Liu, Q.; Kostiainen, M. A.; Linko, V. Robotic DNA Nanostructures. *ACS Synth. Biol.* **2020**, *9* (8), 1923−1940.
(12) Ramezani, H.; Dietz, H. Building Machines with DNA Molecules. *Nat. Rev. Genet.* **2020**, *21* (1), 5−26.
(13) Zhang, Y.; Pan, V.; Li, X.; Yang, X.; Li, H.; Wang, P.; Ke, Y. Dynamic DNA Structures. *Small* **2019**, *15* (26), 1900228.
(14) DeLuca, M.; Shi, Z.; Castro, C. E.; Arya, G. Dynamic DNA Nanotechnology: Toward Functional Nanoscale Devices. *Nanoscale Horiz.* **2020**, *5* (2), 182−201.
(15) Yao, G.; Zhang, F.; Wang, F.; Peng, T.; Liu, H.; Poppleton, E.; Šulc, P.; Jiang, S.; Liu, L.; Gong, C.; Jing, X.; Liu, X.; Wang, L.; Liu, Y.; Fan, C.; Yan, H. Meta-DNA Structures. *Nat. Chem.* **2020**, *12* (11), 1067−1075.
(16) Cao, S.; Wang, F.; Wang, L.; Fan, C.; Li, J. DNA Nanotechnology-Empowered Finite State Machines. *Nanoscale Horiz.* **2022**, *7* (6), 578−588.
(17) Qi, M.; Ma, W.; Xu, Q.; Wang, F.; Song, P.; Jia, S.; Zuo, X.; Li, M.; Yao, G.; Fan, C. Meta-DNA Strand Displacement for Sub-Micron-Scale Autonomous Reconfiguration. *J. Am. Chem. Soc.* **2023**, *145* (30), 16812−16820.
(18) Zhao, Y.; Cao, S. T.; Wang, Y.; Li, F.; Lin, L. X.; Guo, L. J.; Wang, F.; Chao, J.; Zuo, X. L.; Zhu, Y.; Wang, L. H.; Li, J.; Fan, C. H. A Temporally Resolved DNA Framework State Machine in Living Cells. *Nat. Mach. Intell.* **2023**, *5* (9), 980−990.
(19) Douglas, S. M.; Bachelet, I.; Church, G. M. A Logic-Gated Nanorobot for Targeted Transport of Molecular Payloads. *Science* **2012**, *335* (6070), 831−834.
(20) Li, S.; Jiang, Q.; Liu, S.; Zhang, Y.; Tian, Y.; Song, C.; Wang, J.; Zou, Y.; Anderson, G. J.; Han, J.-Y.; Chang, Y.; Liu, Y.; Zhang, C.; Chen, L.; Zhou, G.; Nie, G.; Yan, H.; Ding, B.; Zhao, Y. A DNA Nanorobot Functions as a Cancer Therapeutic in Response to a Molecular Trigger in Vivo. *Nat. Biotechnol.* **2018**, *36* (3), 258−264.
(21) Yin, J.; Wang, S.; Wang, J.; Zhang, Y.; Fan, C.; Chao, J.; Gao, Y.; Wang, L. An Intelligent DNA Nanodevice for Precision Thrombolysis. *Nat. Mater.* **2024**, *23* (6), 854−862.
(22) Uversky, V. N. Introduction to Intrinsically Disordered Proteins (Idps). *Chem. Rev.* **2014**, *114* (13), 6557−6560.
(23) Dawson, R.; Müller, L.; Dehner, A.; Klein, C.; Kessler, H.; Buchner, J. The N-Terminal Domain of P53 Is Natively Unfolded. *J. Mol. Biol.* **2003**, *332* (5), 1131−1141.
(24) Bah, A.; Forman-Kay, J. D. Modulation of Intrinsically Disordered Protein Function by Post-Translational Modifications. *J. Biol. Chem.* **2016**, *291* (13), 6696−6705.
(25) Wicky, B. I. M.; Shammas, S. L.; Clarke, J. Affinity of Idps to Their Targets Is Modulated by Ion-Specific Changes in Kinetics and Residual Structure. *Proc. Natl. Acad. Sci. U. S. A.* **2017**, *114* (37), 9882−9887.
(26) Vassilev, L. T.; Vu, B. T.; Graves, B.; Carvajal, D.; Podlaski, F.; Filipovic, Z.; Kong, N.; Kammlott, U.; Lukacs, C.; Klein, C.; et al. In Vivo Activation of the P53 Pathway by Small-Molecule Antagonists of Mdm2. *Science* **2004**, *303* (5659), 844−848.
(27) Jungmann, R.; Liedl, T.; Sobey, T. L.; Shih, W.; Simmel, F. C. Isothermal Assembly of DNA Origami Structures Using Denaturing Agents. *J. Am. Chem. Soc.* **2008**, *130* (31), 10062−10063.
(28) Zhang, Z.; Song, J.; Besenbacher, F.; Dong, M.; Gothelf, K. V. Self-Assembly of DNA Origami and Single-Stranded Tile Structures at Room Temperature. *Angew. Chem., Int. Ed.* **2013**, *52* (35), 9219−9223.
(29) Bae, W.; Kim, K.; Min, D.; Ryu, J.-K.; Hyeon, C.; Yoon, T.-Y. Programmed Folding of DNA Origami Structures through Single-Molecule Force Control. *Nat. Commun.* **2014**, *5* (1), 5654.
(30) Gállego, I.; Grover, M. A.; Hud, N. V. Folding and Imaging of DNA Nanostructures in Anhydrous and Hydrated Deep-Eutectic Solvents. *Angew. Chem., Int. Ed.* **2015**, *54* (23), 6765−6769.
(31) Rossi-Gendron, C.; El Fakih, F.; Bourdon, L.; Nakazawa, K.; Finkel, J.; Triomphe, N.; Chocron, L.; Endo, M.; Sugiyama, H.; Bellot, G.; Morel, M.; Rudiuk, S.; Baigl, D. Isothermal Self-Assembly of Multicomponent and Evolutive DNA Nanostructures. *Nat. Nanotechnol.* **2023**, *18* (11), 1311−1318.
(32) Zhang, C.; Yuan, Y.; Wu, K.; Wang, Y.; Zhu, S.; Shi, J.; Wang, L.; Li, Q.; Zuo, X.; Fan, C.; et al. Driving DNA Origami Assembly with a Terahertz Wave. *Nano Lett.* **2022**, *22* (1), 468−475.
(33) Zhang, C.; Jing, X.; Guo, L.; Cui, C.; Hou, X.; Zuo, T.; Liu, J.; Shi, J.; Liu, X.; Zuo, X.; Li, J.; Chang, C.; Fan, C.; Wang, L. Remote Photothermal Control of DNA Origami Assembly in Cellular Environments. *Nano Lett.* **2021**, *21* (13), 5834−5841.
(34) Wang, J.; Wei, Y.; Zhang, P.; Wang, Y.; Xia, Q.; Liu, X.; Luo, S.; Shi, J.; Hu, J.; Fan, C.; Li, B.; Wang, L.; Zhou, X.; Li, J. Probing Heterogeneous Folding Pathways of DNA Origami Self-Assembly at the Molecular Level with Atomic Force Microscopy. *Nano Lett.* **2022**, *22* (17), 7173−7179.
(35) Praetorius, F.; Kick, B.; Behler, K. L.; Honemann, M. N.; Weuster-Botz, D.; Dietz, H. Biotechnological Mass Production of DNA Origami. *Nature* **2017**, *552* (7683), 84−87.
(36) Dannenberg, F.; Dunn, K. E.; Bath, J.; Kwiatkowska, M.; Turberfield, A. J.; Ouldridge, T. E. Modelling DNA Origami Self-Assembly at the Domain Level. *J. Chem. Phys.* **2015**, *143* (16), 165102.
(37) Snodin, B. E. K.; Randisi, F.; Mosayebi, M.; Šulc, P.; Schreck, J. S.; Romano, F.; Ouldridge, T. E.; Tsukanov, R.; Nir, E.; Louis, A. A.; Doye, J. P. K. Introducing Improved Structural Properties and Salt Dependence into a Coarse-Grained Model of DNA. *J. Chem. Phys.* **2015**, *142* (23), 234901.
(38) Majikes, J. M.; Patrone, P. N.; Kearsley, A. J.; Zwolak, M.; Liddle, J. A. Failure Mechanisms in DNA Self-Assembly: Barriers to Single-Fold Yield. *ACS Nano* **2021**, *15* (2), 3284−3294.
(39) Arbona, J. M.; Aime, J. P.; Elezgaray, J. Cooperativity in the Annealing of DNA Origamis. *J. Chem. Phys.* **2013**, *138* (1), 015105.
(40) Cumberworth, A.; Frenkel, D.; Reinhardt, A. Simulations of DNA-Origami Self-Assembly Reveal Design-Dependent Nucleation Barriers. *Nano Lett.* **2022**, *22* (17), 6916−6922.
(41) Dunn, K. E.; Dannenberg, F.; Ouldridge, T. E.; Kwiatkowska, M.; Turberfield, A. J.; Bath, J. Guiding the Folding Pathway of DNA Origami. *Nature* **2015**, *525* (7567), 82−86.
(42) DeLuca, M.; Duke, D.; Ye, T.; Poirier, M.; Ke, Y.; Castro, C.; Arya, G. Mechanism of DNA Origami Folding Elucidated by Mesoscopic Simulations. *Nat. Commun.* **2024**, *15* (1), 3015.
(43) Zhang, H.; Wang, Y.; Zhang, H.; Liu, X.; Lee, A.; Huang, Q.; Wang, F.; Chao, J.; Liu, H.; Li, J.; Shi, J.; Zuo, X.; Wang, L.; Wang, L.; Cao, X.; Bustamante, C.; Tian, Z.; Fan, C. Programming Chain-Growth Copolymerization of DNA Hairpin Tiles for in-Vitro Hierarchical Supramolecular Organization. *Nat. Commun.* **2019**, *10* (1), 1006.
(44) Wang, Y.; Lin, H.-X.; Chen, L.; Ding, S.-Y.; Lei, Z.-C.; Liu, D.-Y.; Cao, X.-Y.; Liang, H.-J.; Jiang, Y.-B.; Tian, Z.-Q. What Molecular Assembly Can Learn from Catalytic Chemistry. *Chem. Soc. Rev.* **2014**, *43* (1), 399−411.
(45) Hu, M.; Feng, C.; Yuan, Q.; Liu, C.; Ge, B.; Sun, F.; Zhu, X. Lantern-Shaped Flexible Rna Origami for Smad4Mrna Delivery and

https://doi.org/10.1021/jacsau.5c00195
JACS Au 2025, 5, 1641−1648

Growth Suppression of Colorectal Cancer. *Nat. Commun.* **2023**, *14* (1), 1307.
(46) Guo, L.; Zhang, Y.; Wang, Y.; Xie, M.; Dai, J.; Qu, Z.; Zhou, M.; Cao, S.; Shi, J.; Wang, L.; et al. Directing Multivalent Aptamer-Receptor Binding on the Cell Surface with Programmable Atom-Like Nanoparticles. *Angew. Chem., Int. Ed.* **2022**, *134* (18), No. e202117168.
(47) Cao, S.; Lin, L.; Zhao, Y.; Guo, L.; Zhu, Y.; Wang, L.; Li, J. Programming Aggregate States of DNA Nanorods with Sub-10 Nm Hydrophobic Patterns for Tunable Cell Entry. *JACS Au* **2023**, *3* (4), 1004−1009.

https://doi.org/10.1021/jacsau.5c00195
JACS Au 2025, 5, 1641−1648